Sensors & Actuators: A. Physical 368 (2024) 115117

Contents lists available at ScienceDirect

Sensors and Actuators: A. Physical

journal homepage: www.journals.elsevier.com/sensors-and-actuators-a-physical

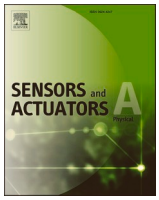

Fiber Bragg grating based displacement sensors with low visual impact for structural health monitoring applications – Monastery of Batalha case

Luís Pereira [a,*], Inês Bourgeois [b], Hugo Rodrigues [b], Humberto Varum [c], Paulo Antunes [a,d]

[a] I3N & Department of Physics, University of Aveiro, Campus Universitário de Santiago, 3810–193 Aveiro, Portugal
[b] RISCO, Department of Civil Engineering, University of Aveiro, Campus Universitário de Santiago, 3810–193 Aveiro, Portugal
[c] CONSTRUCT-LESE, Structural Division, Department of Civil Engineering, Faculty of Engineering, University of Porto, 4200–465 Porto, Portugal
[d] Instituto de Telecomunicações and University of Aveiro, Campus Universitário de Santiago, 3810–193 Aveiro, Portugal

ARTICLE INFO

Keywords:
Fiber Bragg Gratings
Heritage Buildings
Optical Fiber Sensors
Structural Health Monitoring

ABSTRACT

The preservation of heritage structures and buildings is a major concern to guarantee access of the cultural and architectural values to current and future generations. It also contributes significantly to the society in terms of identity, economy, education, and tourism. Due to their ancient nature, combined with the human activity (in and/or around these structures) and the environmental conditions, these structures are particularly susceptible to material deterioration and damage, that can compromise their integrity and the human safety. Therefore, it is crucial the implementation of an adequate monitoring system to analyse the static and dynamic responses of structures. In this paper, we discuss the development and installation of a sensing system for long-term monitoring of crack and joint movements, comprising eight displacement sensing devices and two temperature sensors, in the Monastery of Batalha, Portugal. The displacement sensing devices are formed by transparent small dimension holders and fiber Bragg gratings, with minimal intrusion and very low visual impact. They are relatively easy to fabricate, reproduce, and install, being a viable, efficient, and cost-effective alternative for Structural Health Monitoring sensing applications. Furthermore, they present simple design and principle of operation, which contributes to a straightforward installation and operation, and great versatility, as the alternative pre-strain mechanism of these devices allows to easily adjust the distance between the optical fiber holders. The operational performance of the sensing devices was analysed, and the monitoring results obtained during the following months after their installation are presented and discussed. The long-term data gathered by this sensing system can in the future be used to evaluate possible interventions.

1. Introduction

Structural Health Monitoring (SHM) is a management tool in the civil engineering community that comprises different phases and processes, including sensing, data acquisition, data processing, and analysis. The sensing component is typically composed by a network of sensors that measure relevant parameters, where the data information can be used to evaluate the behavior of existing structures, calibrate numerical models, detect anomalies, and assess structural integrity. The detection of damage or anomalies and their continuous monitoring is fundamental to avoid possible catastrophic events, which may comprise material, economic and life losses. Therefore, SHM can be seen as an important procedure of the infrastructure's maintenance. Nowadays, it has become increasingly essential not only to monitor the structures located in extreme environments, but all the weakened structures susceptible to damage. The above is especially true considering the increasingly common severe weather events due to the climate change effects. In this wide range of structures, the heritage and historical building are a major concern, as old and new anomalies must be monitored to be able to perform the adequate interventions to preserve these monuments. Currently, there are various sensing techniques and sensors for SHM applications, and as the information transmission and data acquisition and management evolves, more complex network sensing configurations can be used, and the dissemination and large-scale implementation of SHM systems can become more and more common in today's society [1,2].

In the optical fiber sensing technology, distributed optical fiber sensors (DOFSs) play an important role in SHM applications, especially

* Corresponding author.
E-mail address: lmpereira@ua.pt (L. Pereira).

https://doi.org/10.1016/j.sna.2024.115117
Received 13 July 2023; Received in revised form 5 December 2023; Accepted 3 February 2024
Available online 7 February 2024

in monitoring large structures [3–5]. This type of sensor uses the entire fiber as sensing element, being capable of performing distributed measurements along several kilometers where temperature and strain-based parameters can be measured with good spatial resolution. However, nowadays, the main drawback of the DOFSs is the high costs of the interrogation systems. Another sensing technique with great potential for SHM applications is the fiber Bragg gratings (FBGs), and the development of sensing configurations and sensor prototypes using these gratings has been the main purpose of several research groups worldwide [6–8]. The use of this optical fiber sensing technology is boosted by its well-known advantages, such as the immunity to electromagnetic interference, independence to optical power fluctuations, absence of electricity at the measuring point, small size, lightweight, multiplexing capabilities, possibility to work in reflection, resistance to harsh environments, easy and well-established fabrication methods, etc.

FBG-based extensometers and displacement sensors are in constant development due to the countless usages and applications for this type of sensing device, notably in SHM. These sensors use the strain sensitivity of the gratings to operate and nowadays they can compete with the electrical and mechanical counterparts due to their distinguished features, namely the non-intrusive and multiplexing capabilities. Several prototypes have been developed for multiple applications, either focusing on a higher sensitivity [9,10] or on a higher operational range [11–13]. Also, FBG-based sensors are not restricted to wavelength demodulation since spectral bandwidth and intensity demodulation sensors have also been developed with the capability to be temperature insensitive [14–17]. In addition, various strain and displacement sensors are commercially available [18,19], with multiple sensing solutions suitable for SHM. Despite the immense possibilities related to the existence of sensor devices and prototypes [20,21], in certain circumstances, customized sensing devices and configurations are still needed for specific environments and applications. Most of these sensors are designed for certain applications and sometimes their sensing specifications are not suitable for different measurement requirements, or the customization of the proposed prototype is difficult due to the complexity of the sensing structure design. Another issue is the fact that several displacement sensors are not developed to take advantage of the FBG multiplexing capabilities or are limited to the number of additional sensors which can be monitored with a single fiber, especially the ones based on spectral bandwidth and intensity demodulation.

For crack and joint monitoring, FBG-based displacement sensors can provide important information about the evolution of these structural elements, and consequently about the structure conditions. This is particularly relevant for fatigue cracks, as their growth can result in catastrophic failure. On one hand, the monitoring of crack detection and growth has been done by embedding the FBG strain sensors in the materials before the crack formation, such as in composite materials [22,23], aluminium samples [24–26], stainless steel samples [27,28] and concrete [29–34]. On the other hand, in existing structures, FBG-based displacement sensors are usually employed in strategic locations where cracks are expected to occur or following the formation of the crack, as an analytical method to correlate the expansion and contraction movements with the influence of mechanical forces and temperature, and as a preventive method to provide an early warning about possible structural failure. There are several examples regarding the application of these sensors in different heritage structures and buildings, for joint and/or crack monitoring and sensor performance assessment. Arêde et al. installed multiple linear position and displacement sensors based on FBGs in several joints of a masonry arch bridge in Vila Fria, Portugal, to measure transverse expansion movements of the arches, joint opening and displacements between opposite spandrel walls [35]. Lima et al. designed and installed a monitoring system with reduced visual impact in the church of Santa Casa da Misericórdia of Aveiro, comprising 19 FBG-based displacement sensors and 5 FBG-based temperature sensors, distributed in key points of the building where important deformations were found or/and would be expected [36]. Felli et al. investigated a crack on the equestrian statue of Bartolomeo Colleoni in Venice, using an array of FBG sensors with the aim of monitoring it during the monument restoration [37]. Coricciati et al. developed smart patches with FBGs embedded and smart rebars with optical time-domain reflectometer-based sensors embedded for SHM of the Monastery in Sant'Angelo d'Ocre, to evaluate the stress/strain state of the renovated structures and their response to seismic events [38]. Verstrynge et al. analysed and compared the performance of semi-distributed FBG-based sensors with other monitoring techniques for crack measurements in a masonry wall [39]. The results proved that the FBGs were effective in monitoring these damages and, in addition, they presented the highest sensitivity and robustness. Alexakis et al. installed an FBG-based sensor network on the March Lane viaduct in Leeds, to monitor surface strains after repair work was conducted in this XIX century structure [40]. The obtained results from the sensors were in agreement with the observed damages, namely the formation of new micro-cracks in the bricks. Bellagamba et al. applied FBG-based sensors to evaluate the long-term crack propagation and the damage evolution at selected locations on the Aurelian Walls in Rome, and to calibrate the parameters used in numerical models [41]. Gupta et al. studied the variations of strain of a brick masonry semi-circular arch which was subjected to settlement at one of its abutments [42]. The FBG-based sensors were mounted on the exterior face of the arch, on adjacent bricks with joints in between considering it tend to crack first.

In this work, we developed and installed a simple and low visual impact sensing layout to monitor crack and joint movements in the historical Monastery of Batalha. The pre-strain mechanism of the displacement sensing devices allows to easily adjust the distance between the optical fiber holders (gauge length), before fixing the fiber to them, permitting the correlation between the displacement sensitivity and the operational range. In addition, these ready-to-install devices allow a simple and effective application on flat surfaces, and since the fiber supports are made of polycarbonate, they are almost transparent and unnoticeable. With this sensing system, we performed sporadic discrete measurements and continuous monitoring over specific time spans in order to evaluate the structural movements. Future long-term monitoring with these sensing devices can be conducted to assess the structural health of those locations of the monument.

2. Monastery of Batalha: background and damage detection

The Monastery of Batalha is a UNESCO World Heritage Site of historical and architectural value, as it is the most representative Gothic building in the country (see Fig. 1(a)), built after the Portuguese victory over the Spanish in the Battle of Aljubarrota, in 1385, which guaranteed Portugal's independence. The monastery is made up of religious (church and chapels) and functional (cloisters and galleries) parts, and its main building material is limestone [43]. The construction of the monastery lasted more than two centuries, and, throughout its time, it experienced some damage, losses and changes caused by earthquakes (1755 and 1969) and the French invasions [44].

Recently, during the inspection of the King Afonso V cloister, it was possible to identify some critical points in the structure, which have been referred for monitoring. The King Afonso V cloister is an element of the Monastery of Batalha that was built in the second half of the XV century. It has two floors, four galleries and is vaulted over a crossing with two ogives. Its single-slope roof was made of tiles and wood, but more recently concrete beams were introduced. The selected critical points were cracks and joint openings where relatively large movements had occurred in the structure at some point (see Fig. 1(b)), and which needed to be monitored in order to understand the stability of these movements prior to the conservation and reparation works:

1. The first critical point is a crack in the masonry wall on the second floor of the cloister, which goes from the top to the floor below.

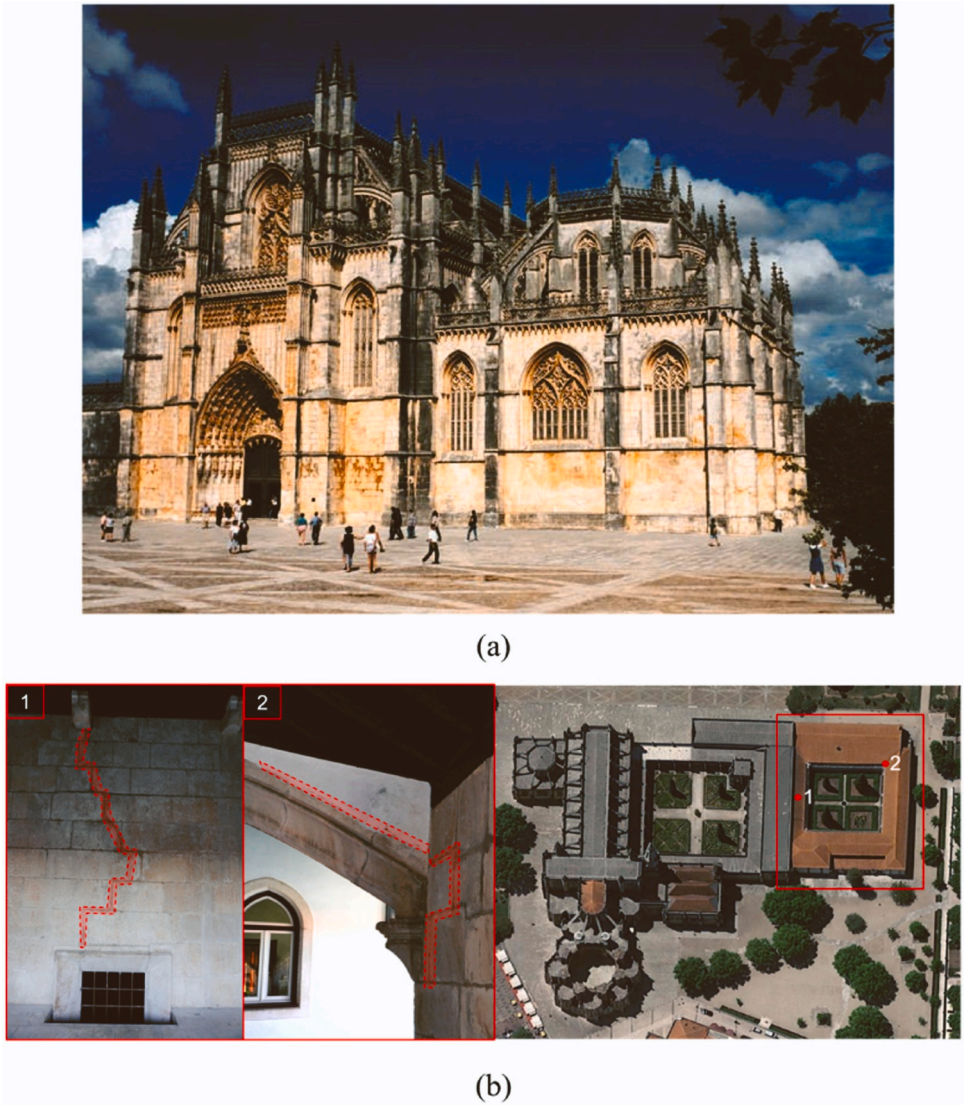

Fig. 1. (a) Monastery of Batalha (archive image); (b) Critical points referenced for monitoring and their location in the cloister of King Afonso V.

2. The second critical point is a pillar on the second floor, which has experienced cracks in the connection points between elements (arch vs pilar) and some joint openings.

The need to monitor the movements of these points, as the monastery is a classified heritage site, led to the implementation of a system that could provide these answers without causing visual impact or damage to the elements and, at the same time offer accurate data that could assist in the diagnostical process. The aim was to understand whether the crack and the joints had stabilised or whether they were experiencing movement, and if they were experiencing movement, whether it was a structural cause or whether it was due to thermal variations.

3. Sensing system description

3.1. FBG inscription

FBG is a periodic (or quasi-periodic) modulation of the refractive index along the core of the optical fiber and a passive wavelength reflecting optical component, which reflects a specific spectral band centered at the Bragg wavelength (λ_B). When a broadband signal is guided through the fiber, the FBG will selectively reflect the wavelength that meets the Bragg condition [45]:

$$\lambda_B = 2n_{eff}\Lambda, \tag{1}$$

where n_{eff} represents the effective refractive index of the core and Λ the period of the refractive index modulation. For sensing applications, the FBGs demonstrate great potential and have been widely used as sensors during the last decades. Any strain or temperature variations applied to the fiber changes both n_{eff} and Λ of the grating leading to a shift in the λ_B. Since the FBG is sensitive both to strain and temperature changes, the λ_B shifts according to:

$$\Delta\lambda_B = 2\left(\Lambda\frac{\partial n_{eff}}{\partial z} + n_{eff}\frac{\partial\Lambda}{\partial z}\right)\Delta\varepsilon + 2\left(\Lambda\frac{\partial n_{eff}}{\partial T} + n_{eff}\frac{\partial\Lambda}{\partial T}\right)\Delta T \tag{2}$$

where $\Delta\varepsilon$ and ΔT are strain and temperature variations, respectively.

The FBGs were produced in GF1AA optical fiber (Thorlabs) with the 266 nm wavelength radiation from a pulsed Q-switched Nd:YAG laser system (LOTIS TII LS-2137 U Laser). More information about the inscription setup can be found in [46,47]. The inscription of each grating was performed through the phase mask technique, using 25 J of pump energy for 5 min, with a pulse repetition rate of 10 Hz. The 8 mm laser beam diameter allowed to inscribe FBGs with 8 mm in length, and the signal from the gratings was monitored in reflection by a Luna HYPERION si155 optical fiber interrogator (during the inscription and later

during the calibration and structural monitoring). In two different fibers, an array of five FBGs were produced in each one, with the proximate λ_B of 1526, 1532, 1541, 1547 and 1555 nm, as Fig. 2 shows. The reason to produce the FBG-based sensors in two different fibers is related to the fact that each sensor array would be installed in separate locations and at different times (and due to the capability of the interrogator to provide measurements in four parallel channels). Each fiber is composed by four displacement sensing devices, F1D1, F1D2, F1D3 and F1D4 in optical fiber 1 (F1) and F2D1, F2D2, F2D3 and F2D4 in optical fiber 2 (F2), and one FBG-based temperature sensor, F1T in optical fiber 1 and F2T in optical fiber 2, for both temperature compensation and readings.

3.2. Sensing device design and deployment

Each displacement sensing device is composed by 2 small fiber holders, designed to hold the fiber strained with the aid of stainless-steel rod with 3 mm in diameter. In order to cause the minimal visual impact and intrusion, the fiber holders, which act as anchorage points for the FBG sensor, are made entirely of polycarbonate material. Although it presents limited chemical resistance to several substances, the polycarbonate is a lightweight and durable material with good mechanical toughness, high impact strength and high glass transition temperature when compared to other thermoplastics [48–50]. In addition, the amorphous polycarbonate has excellent transparency in the visible spectral range [49,51]. Details of the polycarbonate fiber holder is presented in Fig. 3(a). Each holder is 10 mm in length, 10 mm in width and 5 mm in height. A hole with 3 mm in diameter goes through the holder (to insert a stainless-steel rod), parallel with the fiber groove on the top and perpendicular to another hole machined with a female thread to incorporate a M3 hex socket plain end cup screw. In each displacement sensing device, the stainless-steel rod goes through two holders, allowing their alignment, to apply the optical fiber, and control over the sensing length, at which point the M3 screws fix the holders in the desired position on the rod and all parts of the device become united and steady (see Fig. 3(b)). The acrylate coating of the optical fiber containing the FBG is removed along the fiber sensing length (distance between the two holders) and an additional 5 mm corresponding to half the length of the groove in each holder, to guarantee that the fiber does not slip once it is glued to the holder. Then, the optical fiber is placed in the grooves, strained and glued to the holders with Araldite epoxy, according to Fig. 3(c). In the final stage, after the sensing device has been applied to the area to be monitored (and the holders have been attached to the surface), the M3 screws are loosened, and the stainless-steel rod is removed. The result, depicted in Fig. 3(d), is an FBG-based sensor strained, able to measure increase or decrease displacement movements, composed only by the optical fiber and the polycarbonate holders at the anchorage points, making this transparent sensing configuration almost unnoticeable and unintrusive.

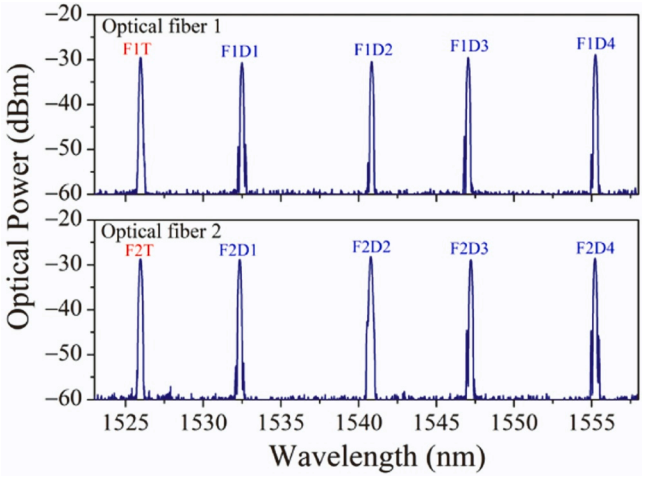

Fig. 2. Reflection spectra of the inscribed FBGs in two different optical fibers and their identification in the upcoming sensing configuration.

3.3. Sensors characterization

3.3.1. Strain/displacement

The design of this sensing device allows to freely control the relationship between the displacement sensitivity (S_D) and the operational limit (O_L). Here, the O_L is considered the operational range of the displacement sensing devices, that is, comprises displacement values that correspond to the amount of applied strain in the optical fiber, from 0 με up to the average strain limit (breakage point). An increase in one of previous parameters implies a decrease in the other, and consequently they can be adjusted according to the necessary requirements set for a specific application. In order to obtain a viable characterization of the displacement sensing devices, the strain responses and limits of the GF1AA fiber samples containing FBGs were studied. The setup employed in these tests is illustrated in Fig. 4.

First, the acrylate coating of the optical fibers, along the sensing length, was stripped (according to the description of the displacement sensing device in Section 3.2) and the fibers were attached between a fixed stage and a three-axis manual translation stage, with 10 μm resolution. Twelve identical optical fiber samples with FBGs inscribed, with a λ_B around 1555 nm (see Fig. 4), were used in this strain test, and with steps of 500 με and a stabilization time of one minute, each fiber was stretched until breakage. Fig. 5(a) shows the strain sensitivity of each sample, where the values varied between 1.14 pm/με and 1.20 pm/με and the obtained average strain sensitivity was 1.17 pm/με. On the other hand, Fig. 5(b) presents the corresponding strain limit for each fiber sample, showing that the minimum strain value at which the fiber broke was 5000 με and the maximum value was 10000 με, with an average strain limit of 6942 με.

With the previous results, the sensitivity and the approximate operational range of the displacement sensing device can be obtained according to the effective sensing length or distance between the polycarbonate fiber holders (L), as Fig. 6 shows. The approximate O_L was obtained using the average strain limit from Fig. 5(b), and can be described by the following expression:

$$O_L(mm) = 0.006942 \times L(mm), \tag{3}$$

while the S_D was achieved through the average strain sensitivity from Fig. 5(a), and represented by:

$$S_D(pm/\mu m) = \frac{1170}{L(mm)} \tag{4}$$

The previous equations and Fig. 6 demonstrate that the L will determinate both S_D and O_L, as the L approaches the shorter values, the higher is the S_D and more limited is the working range of the sensing device. Therefore, for applications where high sensitivity is required in relatively small displacement environments, small L values are recommended, while in applications where it is expected to occur large displacement movements, higher L values are needed to avoid a possible failure of sensing device.

3.3.2. Temperature

Each FBG array contains a grating to monitor temperature variations in that area. The purposes of these sensors are to address the strain/temperature cross sensitivity of the displacement sensing devices and to simultaneously obtain temperature readings. Therefore, the thermal response of these gratings was studied by placing them in a climate chamber (model L C/64/70/3, Weiss Technik LabEvent). Three thermal cycles were performed, where in each cycle the temperature was increased from 5 °C to 40 °C, and then decreased back to 5 °C, using steps of 5 °C and a stabilization time of 30 min. Figs. 7(a) and 7(c) show

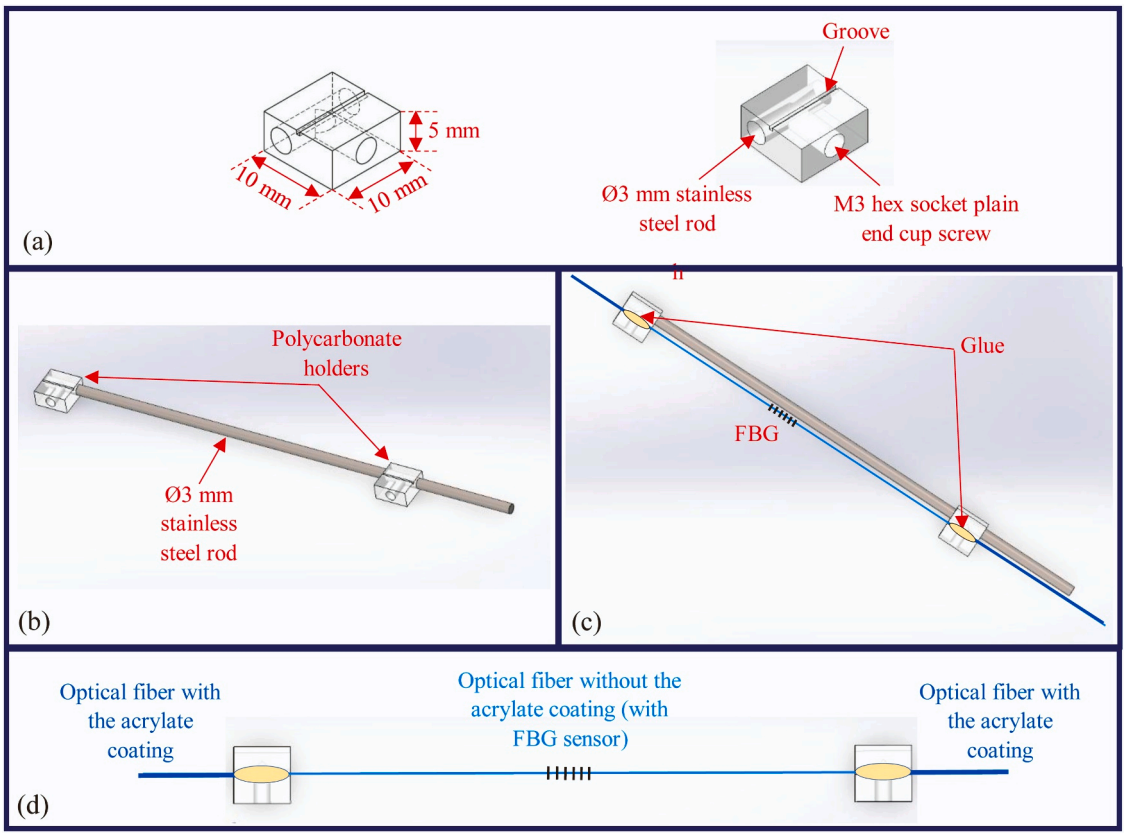

Fig. 3. (a) Details of the polycarbonate fiber holder; (b) Apparatus of the displacement sensing device without the FBG sensor; (c) Ready-to-install displacement sensing device with a pre-stained FBG glued to the polycarbonate holders; (d) Final result of the sensor after the installation.

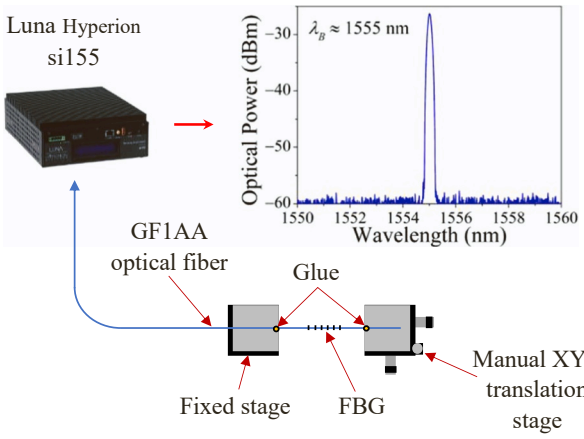

Fig. 4. Scheme of the setup to characterize the strain performance of the GF1AA samples containing FBGs. The inserted reflection spectrum is from the first sample.

the λ_B variation during the first cycle for F1T and F2T, respectively. After linearization, the temperature sensitivities (S_T) were 8.56 ± 0.06 pm/°C (increase) and 8.67 ± 0.03 pm/°C (decrease) for F1T, 8.75 ± 0.05 pm/°C (increase) and 8.89 ± 0.03 pm/°C (decrease) for F2T. With the obtained data, these temperature sensors can be calibrated for temperature measurements through the following linear equation:

$$T(^{\circ}\mathrm{C}) = a \times \lambda_B + b, \tag{5}$$

Where a and b are the slope and yy intercept, respectively. Figs. 7(b) and 7(d) show the linearization when temperature varies in function of the λ_B, for F1T and F2T respectively, in the first thermal cycle. The S_T, a, and b results for the three thermal cycles are summarized in Table 1. The S_T varied between 8.56 and 8.81 pm/°C (0.25 pm/°C difference) and between 8.70 and 8.97 pm/°C (0.27 pm/°C difference), for F1T and F2T respectively. Concerning the temperature readings, the average of the a and b values from the three cycles was obtained for both F1T and F2T and used in the temperature measurements by employing Eq. 5.

3.4. Sensors production and installation

The production of the displacement sensing devices was carried out according to the description in Section 3.2. From the previous results, it was first decided to use in this application displacement sensing devices with an L value of 100 mm, which have an S_D of 11.7 pm/μm and an approximate O_L of 0.694 mm, demonstrating a balanced performance between both parameters since it was not expected to register major movements in the cracks and joints. The distance between the polycarbonate holders (see Fig. 8(a)) was initially adjusted and later they were secured to the steel rod by the M3 screws. The following step was fixing this device in a setup between two manual translating stages, which allowed to strain the fibers containing the FBG sensors before attaching them to the polycarbonate holders. This process was repeated eight times, since the sensing network is composed by two FBG arrays, each compressing four displacement sensing devices and one bare FBG-based temperature sensor at the end of the optical fiber (see Fig. 8(b)). The result, depicted in Figs. 8(c) and 8(d), is the production of eight ready-to-install displacement sensing devices.

The installation of the sensing devices occurred on the 13th (F1) and 20th of October (F2), 2022. First, at the sensor's location, the surface of the stones was clean and afterwards the pre-strained displacement sensing devices were attached by employing a beige epoxy (to camouflage even further the presence of these devices). The transparent optical fiber, that links the sensing devices and connects them to the location of

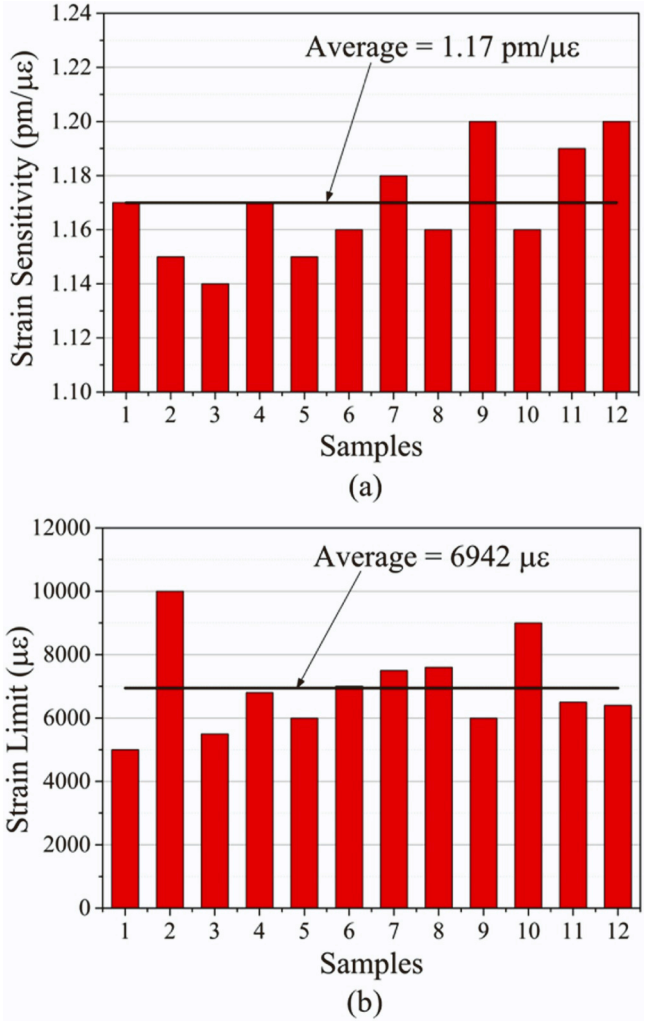

Fig. 5. (a) Strain sensitivities obtained from twelve FBG samples; (b) Corresponding strain limits of the optical fiber samples.

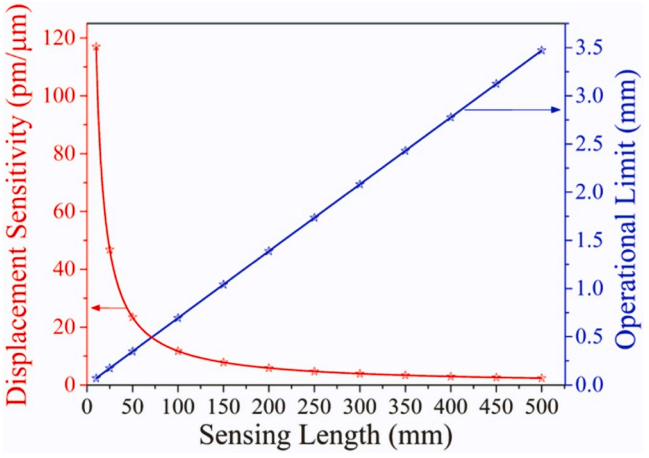

Fig. 6. Relationship between the displacement sensitivity and the sensing length (red) and relationship between the approximate operational limit and the sensing length (blue).

the monitoring equipment, was also attached to the stone walls by the same epoxy. Several hours later, when the epoxy was cured, the pre-strain mechanism was loosened and the steel rod was removed in each device, at which moment the measurement of the displacement began. Figs. 9(a) and 9(b) show an attached sensing device over a crack of interest, right after fixing it to the stone and after the removal of the steel rod, respectively.

The viability of the pre-strain mechanism, and consequently of this ready-to-install displacement sensing device, was analysed by measuring the wavelength variation of the FBG sensors, since their inscription until their installation. Figs. 10(a) and 10(b) present the $\Delta\lambda_B$ of the gratings from F1 and F2, respectively, at different moments until their installation, at which point the pre-strain mechanism was loosened and the steel rod removed. After their inscription, the FBGs, that will act as displacement sensors, were randomly stretched up to strain values between approximately 600 and 800 με and then fixed to the polycarbonate holders. From the day these displacement sensing devices were produced (strained and fixed to the holders) to the day they were installed (before installation), the strain decreased in all sensors, to values between 480 (F2D1) and 630 με (F1D4). This can be explained by the fact that the holders (together with the steel rod) were fixed while the strained optical fibers (containing the FBGs) were glued to them, and therefore, they were subjected to additional stress during this process, which was reduced after the removal of these devices from the setup. It should also be noted that these displacement sensing devices were produced three months before their installation, and during that time the pre-strain mechanism maintained the fibers stretched. The $\Delta\lambda_B$, and consequently the strain variation after attaching the devices to the walls, is affected by the characteristics of the stone surface, namely if it is smooth or irregular and rough. In this case, these characteristics were dependent on the sensors' locations, as the strain variation during this process was not uniform, since it increased in two sensing devices (F1D3 and F2D4) and decreased in the others. In the final step, after loosening the pre-strain mechanism and removing the steel rod, the strain level decreased slightly in all devices. Nevertheless, the FBGs of all displacement sensing devices were under strain after the installation, between 320 με (F2D1 and F2D2) and 600 με (F2D4), demonstrating the viability of this pre-strain mechanism and showing that this ready-to-install displacement sensing device has great potential to be employed in SHM applications. The FBG-based temperature sensors, F1T and F2T, were unstrained and only subjected to temperature variations. Consequently, their $\Delta\lambda_B$ is much more reduced when compared with the strained displacement sensing devices.

Later, after several weeks since the installation of this sensing system, new displacement sensing devices with an L value of 250 mm were produced and installed to substitute the ones damaged by the large displacement movements. According to Eqs. 3 and 4, devices with L = 250 mm have an S_D of 4.7 pm/μm and an O_L of approximately 1.736 mm.

The disposition and location of the installed displacement sensing devices from F1 and F2 are presented in Figs. 11 and 12, respectively. The devices from F1 are positioned in a vertical crack, that travels along the stone blocks and joints, located at consecutive stone block layers. Sensing devices F1D1 and F2D2 cover the crack in two consecutive stone blocks, while F1D3 monitors the joint above them and lastly, F1D4 monitors both the crack and the joint in an upper position. The temperature sensor F1T is located in the middle of the stone wall, next to F1D1. On the other hand, the sensing devices from F2 are located and dispersed on both sides of a corner (see Fig. 12), where they are monitoring different points of interest, in which the cement had previously deteriorated and fallen due to possible movements and tension between the stone blocks.

4. Results and discussion

The monitoring of both temperature and displacement movements was conducted at different periods, by both discrete and continuous measurements. The discrete measurements did not follow a scheduled pattern, but an attempt was made to have one reading per month. The

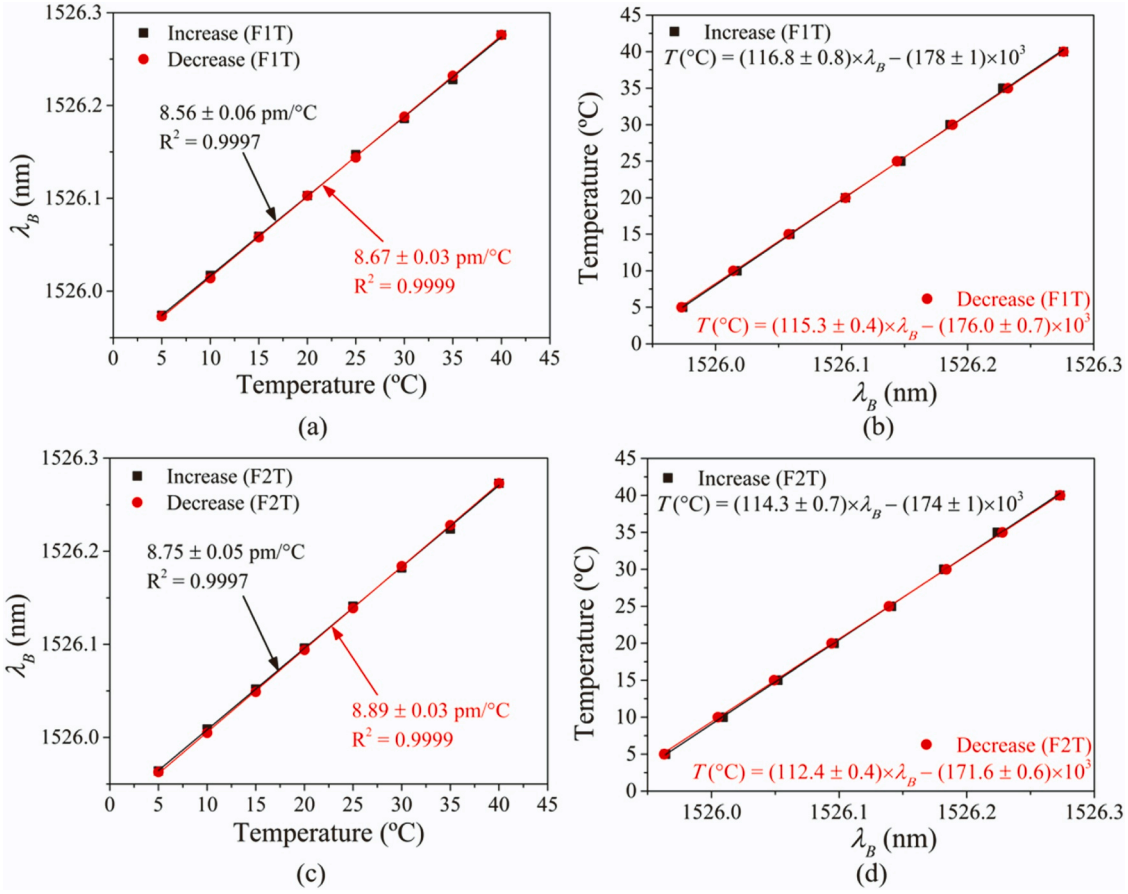

Fig. 7. (a) F1T λ_B variation with the increasing/decreasing temperature; (b) Corresponding temperature readings in function of λ_B; (c) F2T λ_B variation with the increasing/decreasing temperature; (d) Corresponding temperature readings in function of λ_B.

Table 1
Results of the calibration parameters, obtained from the 3 thermal cycles, for F1T and F2T.

Thermal Cycle	a (°C/nm) F1T	Average (°C/nm)	b (10^3 °C)	Average (10^3 °C)	S_T (pm/°C)
1 (increase)	116.8	115.1	–178.3	–175.7	8.56
1 (decrease)	115.3		–176.0		8.67
2 (increase)	113.4		–173.1		8.81
2 (decrease)	113.7		–173.6		8.79
3 (increase)	116.5		–177.7		8.58
3 (decrease)	115.1		–175.6		8.69
	F2T				
1 (increase)	114.3	113.1	–174.4	–172.6	8.75
1 (decrease)	112.4		–171.6		8.89
2 (increase)	111.4		–170.0		8.97
2 (decrease)	111.8		–170.6		8.94
3 (increase)	114.8		–175.2		8.70
3 (decrease)	113.9		–173.8		8.77

displacement and temperature values obtained from the discrete measurements are presented in Figs. 13(a) and 13(b), for F1 and F2 arrays, respectively. Due to the unexpected large displacement movements of the crack, where the F1 array was monitoring, the O_L of the displacement sensing devices was possibly surpassed, resulting in their failure at different points in time. Therefore, multiple interventions were made to continue the monitoring of this crack, which included the installation of new devices (with $L = 250$ mm) with the capability to withstand higher displacements. The first one to fail was F1D1, before the third measurement (25 days after installation), when the other active sensing devices registered a rapid displacement increase up to 0.131 mm. The second one to fail was F1D4, when the displacement measured by the remaining devices continued to increase up to 0.221 mm. F1D3 failed on the following measurement and lastly F1D2 failed after more than 81 days since its installation. Since the registered displacement movements were inferior to the O_L of these displacement sensing devices, it can be confirmed that the expansion of the crack during the time span between measurements was far superior to the measured values. Additionally, after installing the new displacement sensing devices to replace the ones that had failed (while F1D2 was still active), an increase in displacement up to 0.130 mm was later registered by these sensors (54 days after their installation). Since the monitored displacement behaviour is almost similar along the crack (see Fig. 13(a)), if F1D2 had endured until that moment, it would show an estimated displacement value of approximately 0.320 mm. Also, note that the measurements after this moment show a continuous displacement decrease from the contraction of the crack, until the FBGs of the new displacement sensing devices became unstrained (after 3rd of April 2023), suggesting that the displacement was much higher when F1D2 failed.

The analysis of the obtained results, from both displacement and temperature sensing devices, suggests that the major crack movements follow wide cycles (several months) and are possibly dependent on the average temperature of the seasons. During November, the displacement increased drastically, when the temperature dropped, and it continued until February, when the displacement started to decrease. Hence, the crack expands as the temperature decreases and reaches its higher expansion during the winter months, possibly due to the shrinkage of the surrounding stone blocks.

On the other hand, the devices from F2 array measured lower displacement movements compared to the previous sensing devices, showing different displacement behaviour of the different monitored

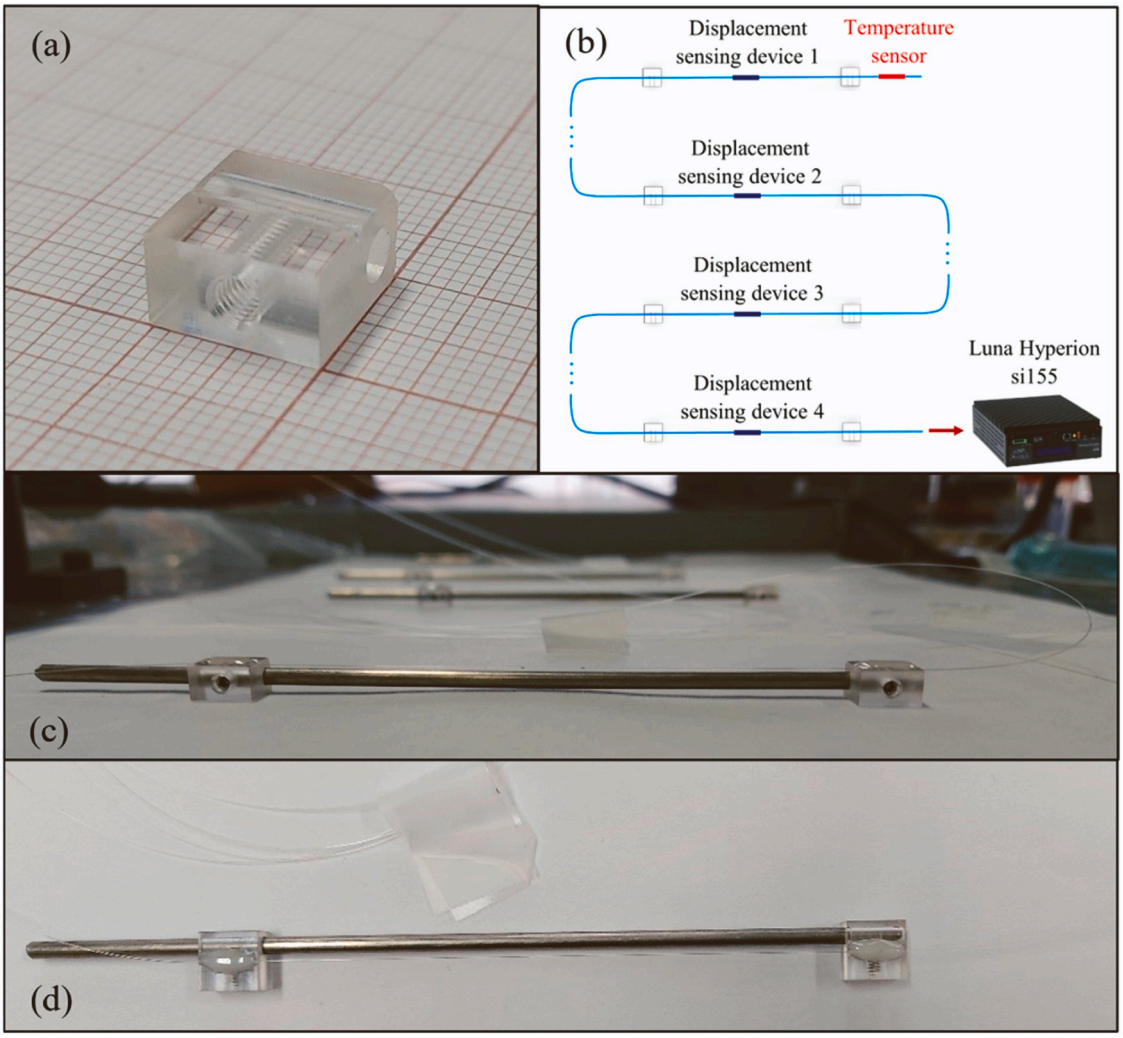

Fig. 8. (a) Picture of the polycarbonate fiber holder; (b) Scheme of the multiplexed sensing configuration and monitoring; (c) Side view of the displacement sensing devices; (d) View from above of the displacement sensing devices.

joints (see Fig. 13(b)). Here, F2D1 and F2D2 presented similar behaviour, especially during the initial measurements, in which the displacement decreased just after the installation of these devices. In the case of F2D1, the displacement measurements were negative during the entire monitoring period. Despite measuring negative displacements for most of the monitoring period, F2D2 began to present higher displacements with the increase of the temperature. Regarding F2D3 and F2D4 sensors, the displacement increased after the installation, and in the case of F2D4 it remained relatively high during the later stage of the monitoring period (after February).

The displacement and temperature information obtained from the continuous measurements are presented in Figs. 14(a) and 14(b), for F1 and F2 arrays, respectively. The continuous measurements occurred between the following days:

1. 23rd of December 2022 and 2nd of January 2023;
2. 15th of February 2023 and 22nd of February 2023;
3. 3rd of April 2023 and 11th of April 2023.

Regarding the F1 sensing devices (see Fig. 14(a)), during the first continuous monitoring period (23 Dec – 2 Jan), the first F1D2 device was still active and consequently, the displacement values were much higher when compared to the remaining displacement sensing devices, which were installed on the 23rd of December to replace the failed ones. Despite the displacement difference between F1D2 and the other devices (around 0.180 mm), all of them registered a similar displacement behaviour and variation during this monitoring period. Between the first and the second (15 Feb – 22 Feb) monitoring periods, F1D2 failed as the newly installed sensing devices registered a significant displacement increase. Due to the profile of the displacement variation during the second monitoring period, which decreases continuously at all sensor locations, F1D1 (from 0.116 to 0.045 mm), F1D3 (from 0.121 to 0.046 mm) and F1D4 (from 0.130 to 0.054 mm), it is most likely that the displacements were much higher before 15th of February.

As mentioned before, the major crack movements follow wide cycles and this second monitoring period occurs during a phase transition, where the crack is continuously contracting. The daily effect of the temperature variation results in minor crack movements (temperature increase leads to the contraction of the crack), which become more significant as the daily thermal variation increases. In the third continuous monitoring period (3 Apr – 11 Apr), due to the significant reduction of the gaps from the crack (because of the higher daily temperatures in this period), all FBGs of the displacement sensing devices were unstrained and consequently unable to monitor any movements during this period. Considering the global analysis of the F1 measurement data, in terms of structural integrity, the crack experienced considerable divergent movements during the cold months, unlike the warm months where the crack almost closed.

The continuous monitoring of the F2 sensing devices occurred in the same periods, and this information is depicted in Fig. 14(b). During the

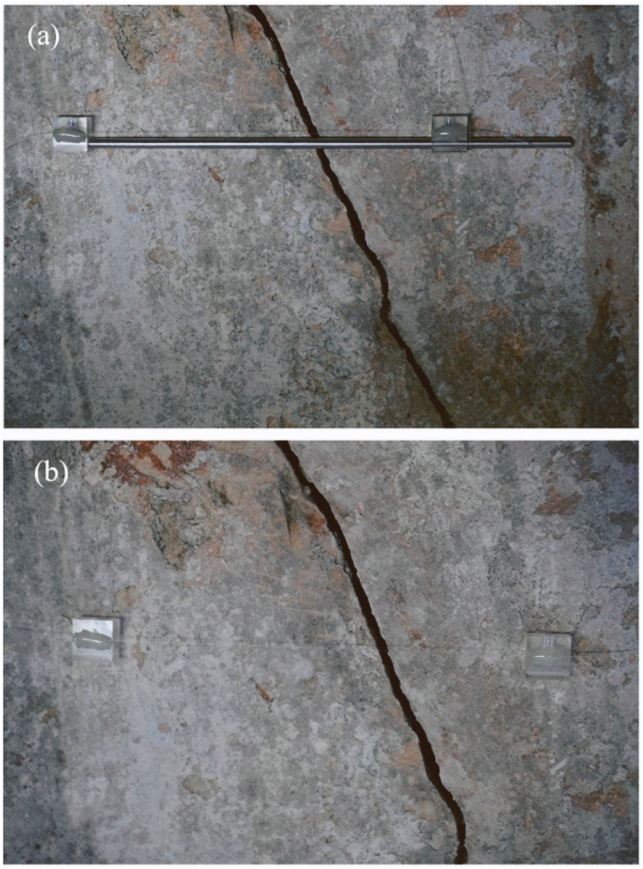

Fig. 9. (a) Displacement sensing device after attaching it to the stone; (b) Same device after the installation.

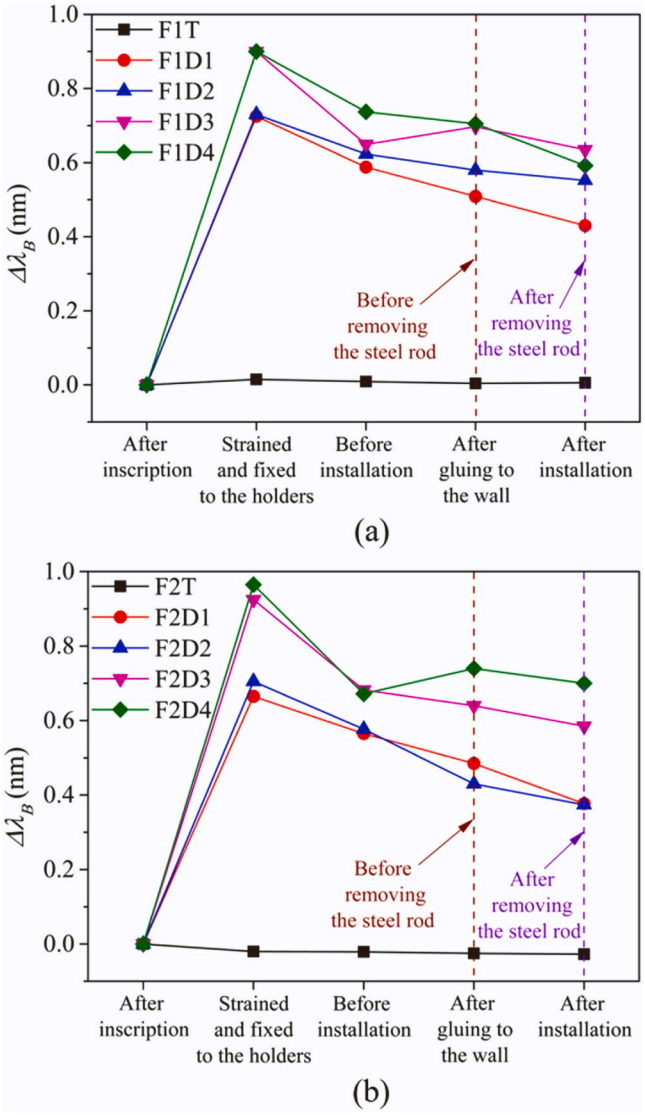

Fig. 10. Wavelength variation of the FBG-based sensors since their inscription until their installation in the Monastery of Batalha: (a) F1 array; (b) F2 array.

first monitoring period, all devices measured relatively minor daily displacement movements, in which F2D1 and F2D2 registered negative displacements while F2D3 and F2D4 registered positive displacements. As the daily temperature variation increases in the following monitoring periods, the displacements become more significant, especially in the third monitoring period. The F2D1 measured negative displacements during the entire monitoring time, where the values varied between –0.007 and –0.016 mm in both the second and third monitoring periods. The displacement registered by F2D2 show a gradual increase as the daily temperature oscillations increase, which is most noticeable during the third monitoring period. The minimum daily displacements measured by this device are located between –0.010 and –0.0014 mm during the entire monitoring time, while the maximum daily displacements, achieved during the second and third monitoring periods, are 0.003 and 0.013 mm, respectively. The displacement registered by F2D3 has a similar profile as F2D2, once the daily displacement variations measured by these sensing devices follow the daily thermal cycles. About the F2D4, the displacement varied between –0.002 and 0.015 mm during the first monitoring period, but in the second and third monitoring periods the displacement increased to values between 0.020 and 0.046 mm. Unlike the other monitored joints, in the F2D4 location, the joint contracts with the increasing temperature.

The major movements observed in F2 sensing devices during these continuous monitoring periods were influenced by the daily temperature variations, and after analysing both thermal and displacement daily cycles, it was noted an approximately two hours delay of the joints movement cycle regarding the air temperature cycle. The amplitude of both the daily displacement and temperature variations measured by the F2 array are presented in Figs. 15(a), 15(b) and 15(c) for the first, second and third monitoring periods, respectively. The displacement variation is determined by the amplitude of the daily temperature variation on most days. For the F2D1, F2D2, and F2D3 devices the displacement variation is positive with the increasing temperature, in which F2D3 presents higher variation during the first monitoring time, while during the remaining monitoring periods F2D2 and F2D3 show a similar dependence on the temperature variation. About the F2D4, the measured displacement variation is negative for a positive temperature variation, as this joint contracts with the increasing temperature. Regarding the structural integrity of the column, after performing the global analysis to the F2 measurement data, is possible to state that the joints suffered small movements that do not compromise the structure.

5. Conclusions

In conclusion, this paper reports the development, characterization, and installation of a simple and low visual impact FBG-based sensing system in the historical Monastery of Batalha, whose purpose is the long-term monitoring of cracks and joints of interest. The developed displacement sensing devices have the capability to adjust, during the production, the gauge length to obtain an adequate O_L and S_D for the application. Since their final setup includes only optical fiber and polycarbonate holders at the anchorage points, they are almost unnoticeable, which is an important characteristic for SHM applications in

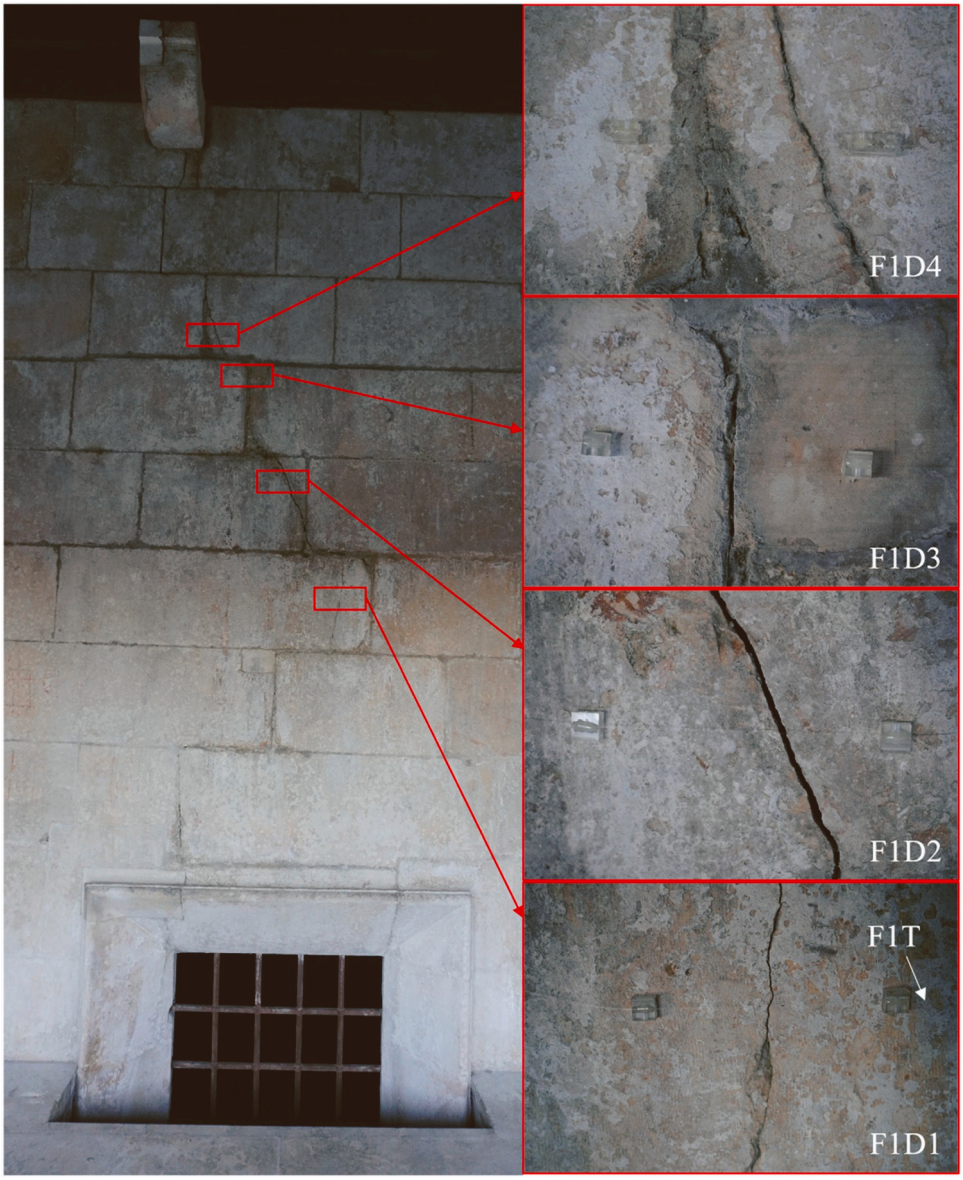

Fig. 11. Displacement sensing devices from F1 after the installation.

heritage structures. When comparing these sensors' capabilities to other existing sensing strategies, they offer a unique combination of sensitivity, reliability, and flexibility. Furthermore, these devices present simple and straightforward operation, are easy to fabricate, reproduce, and install, and are a cost-effective solution for this type of applications. Also, it is important to note that these sensors do not require electrical connections within the structure, unlike traditional electrical sensors, and do not suffer from electrical interference. Also, their multiplexing capabilities provide efficient and cost-effective monitoring of different structural elements.

This sensing system is composed by 10 FBGs multiplexed in two optical fibers, each containing four displacement sensing devices and one FBG-based temperature sensor. After their installation, both discrete and continuous measurements were conducted. The displacement sensing devices from F1 (with a $L = 100$ mm) failed at different moments during the monitoring, due to the unexpected large movements from the crack they were located. They were later substituted by new devices, with $L = 250$ mm to be capable of withstand this kind of movements. During this crack monitoring, the measured displacement reached values up to 0.221 mm, but presumably the displacement was much higher in certain periods between measurements. On the other hand, the sensing devices from F2 were installed in different joints, where the movement behaviour was studied and correlated with the temperature data. These devices registered different movement behaviours from the monitored joints, which were highly affected by the thermal conditions and the daily temperature variations.

It should be highlighted that these displacement sensing devices, particularly the polycarbonate holders design, were produced with reduced dimensions for these specific locations, with flat surfaces. Therefore, these holders can be produced and machined to adapt this device to non-uniform surfaces and/or locations with specific features.

With this application case, it was possible to implement a monitoring system with no visual impact for the building structure and capable of providing precise data of the movements that the structure is experiencing. The approach was to develop a sensing device that would withstand movements in a certain range of values. In this case it was assumed that the movements would be smaller than 0.1 mm, and since this silica optical fiber can withstand strain up to approximately 6942 με of its fixed distance, the initial devices had an O_L of 0.694 mm ($L = 100$ mm). However, when these sensing devices are used, they are pre-

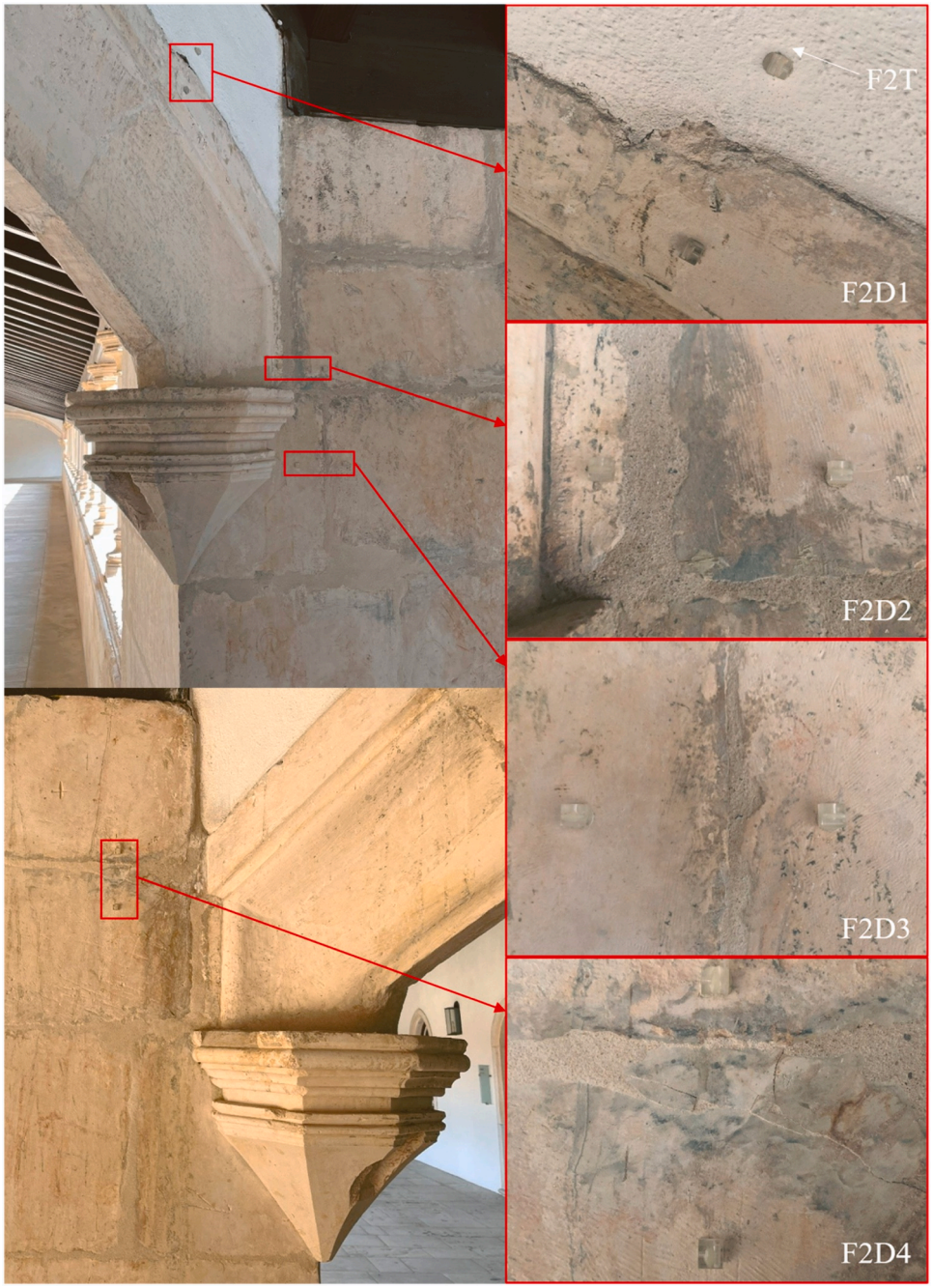

Fig. 12. Displacement sensing devices from F2 after the installation.

strained, and this affects the amount of additional strain the optical fiber can resist. It must be highlighted that the O_L of the sensing device also comprises the pre-strain applied to the FBG, during the production. In the case of the F1 sensing devices, the O_L (which also includes the pre-strain) was insufficient, causing the fibers to break, and it was necessary to implement new devices with an O_L capable of withstanding higher displacements. For the viability of the displacement sensing devices, it is critical that the O_L is one order of magnitude higher than the measured displacement variations. Besides the sensor failure, it is also important to consider the opposite behaviour, when the displacement decreases below the operational range (when the optical fiber becomes unstrained) and the device is unable to detect any displacement. To avoid these situations, a crackmeter could have been installed beforehand to know the magnitude of the movements experienced by the structure and then, devices with the appropriate L (and O_L) could be produced. Alternatively, FBGs in polymer optical fiber (POF) could also be employed for the initial analysis about the movements and/or long-term monitoring. These fibers present better stretching performance and higher strain limits (the displacement sensing devices would present higher O_L and be able to withstand larger movements). However, since most of the polymer materials present high losses in the 1550 nm spectral region, arrays with multiplexed sensing devices would be very difficult to achieve. Thus, only single POF-based devices could be implemented in this application. Nevertheless, the obtained results demonstrate the capability of these non-intrusive displacement sensing devices for long-term monitoring in heritage structures, and the employment of other optical fibers in these devices could be a case of study in the future. Also, since the removal of the acrylate coating of the optical fibers is necessary to inscribe the FBGs (via UV lasers) and fix the fiber to the holders, the recoating of the optical fibers through the

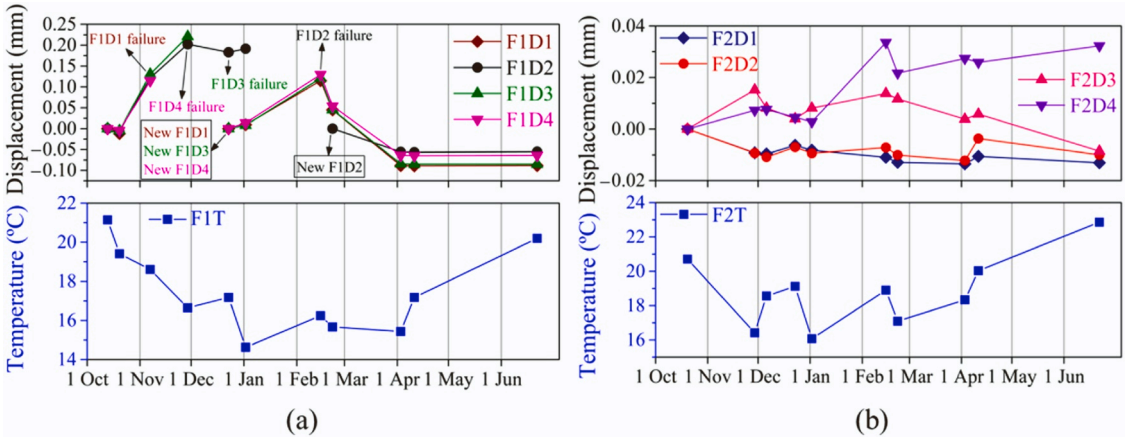

Fig. 13. Displacement and temperature discrete monitoring of: (a) F1 array; (b) F2 array.

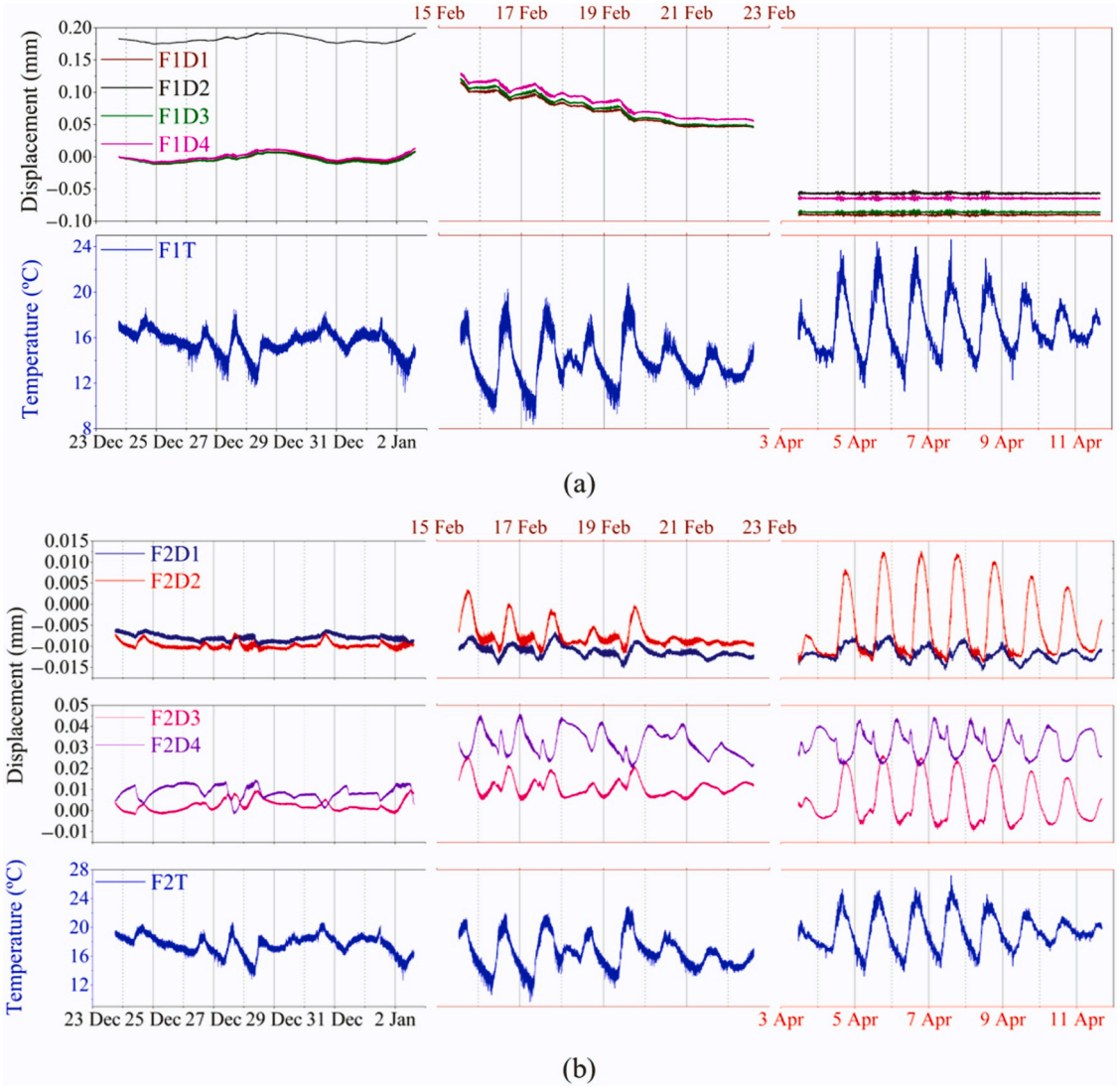

Fig. 14. Displacement and temperature continuous monitoring (between 23 Dec 2022 – 2 Jan 2023 (dates on the bottom), 15 Feb 2023 – 23 Feb 2023 (dates on the top) and 3 Apr 2023 – 11 Apr 2023 (dates on the bottom)) of: (a) F1 array; (b) F2 array.

deposition of elastic and protective polymer materials could be a case of study in the future, to improve the robustness of the fiber and possibly increase the O_L of the sensing devices. On the other hand, gratings could also be inscribed with femtosecond laser systems to avoid the removal of the coating in that section.

In terms of data analysis, it has been shown that: (1) the crack

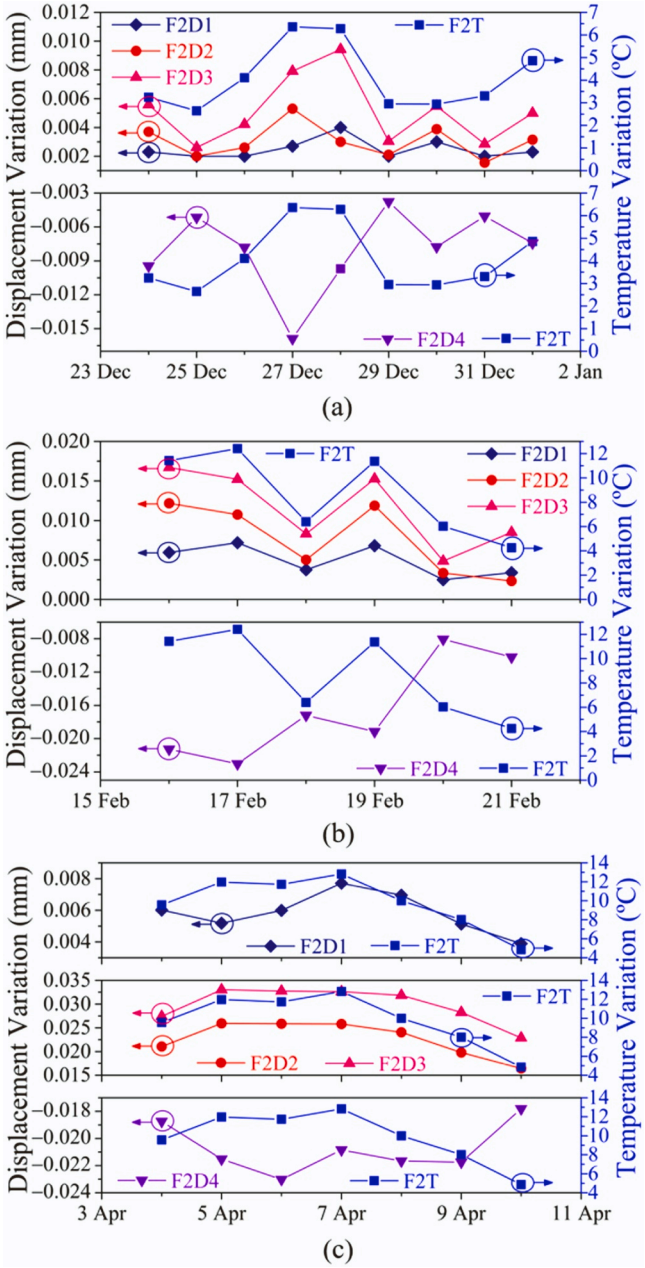

Fig. 15. Daily temperature and displacement variations from the F2 array during: (a) First continuous monitoring period (24 Dec 2022 – 1 Jan 2023); (b) Second continuous monitoring period (16 Feb 2023 – 21 Feb 2023; (c) Third continuous monitoring period (4 Apr 2023 – 10 Apr 2023).

experiences divergent movements in the cold months and closes in the warm months. This phenomenon can be related to the groundwater level (combined with the fact that this wall is protected from the sunlight), but more data on the cold months will be needed to understand if the crack behaves in the same way; (2) the joints of the column have experienced small order movements, suggesting that there has been a stabilisation of the movements that had previously caused the joint material to fall.

Nowadays, for preservation purposes, the cracks and joints monitoring is necessary to analyse the structural stress level and is an important tool to assess their evolution through time and evaluate possible interventions to avoid catastrophic damages and failures. Therefore, the use of this sensing system is not only essential to study the behaviour of historic buildings and structures, but also to monitor strategic, faulty and/or damaged structural features for long periods of time. With this in mind, future long-term monitoring with these sensors will continue to be conducted to assess the structural heath in those locations of the monument. Furthermore, new displacement sensing devices, with the same design and characteristics, will be installed in other critical locations of this national monument, which will help even further the preservation of this heritage building.

CRediT authorship contribution statement

Pereira Luis: Formal analysis, Investigation, Methodology, Resources, Visualization, Writing – original draft. **Bourgeois Inês:** Conceptualization, Investigation, Methodology, Writing – review & editing. **Rodrigues Hugo:** Conceptualization, Methodology, Project administration, Writing – review & editing. **Varum Humberto:** Writing – review & editing. **Antunes Paulo:** Conceptualization, Methodology, Project administration, Resources, Supervision, Writing – review & editing.

Declaration of Competing Interest

The authors declare that they have no known competing financial interests or personal relationships that could have appeared to influence the work reported in this paper.

Data availability

Data will be made available on request.

Acknowledgments

This work was funded by FCT/MCTES through national funds and, when applicable, cofunded by EU funds under the projects UIDB/50008/2020-UIDP/50008/2020, UIDB/50025/2020, and UIDP/50025/2020. It was also supported by FCT/MEC through national funds and cofunded by a FEDER-PT2020 partnership agreement under the project UID/EEA/50008/2019. Luís Pereira acknowledges FCT for the grant with reference SFRH/BD/146295/2019. Inês Bourgeois acknowledges FCT for the grant with reference PRT/BD/152876/2021.

References

[1] S.C. Mukhopadhyay, New Developments in Sensing Technology for Structural Health Monitoring, in: Lecture Notes in Electrical Engineering, volume 96, Springer, 2011.
[2] S. Aleksic, A survey on optical technologies for IoT, smart industry, and smart infrastructures, J. Sens. Actuator Netw. vol. 8 (3) (2019) 47.
[3] A. Barrias, G. Rodriguez, J.R. Casas, S. Villalba, Application of distributed optical fiber sensors for the health monitoring of two real structures in Barcelona, Struct. Infrastruct. Eng. vol. 14 (7) (2018) 967–985.
[4] M.F. Bado, J.R. Casas, A review of recent distributed optical fiber sensors applications for civil engineering structural health monitoring, Sensors vol. 21 (5) (2021) 1818.
[5] H. Wijaya, P. Rajeev, E. Gad, Distributed optical fibre sensor for infrastructure monitoring: Field applications, Opt. Fiber Technol. vol. 64 (2021) 102577.
[6] J.M. López-Higuera, L.R. Cobo, A.Q. Incera, A. Cobo, Fiber optic sensors in structural health monitoring, J. Light. Technol. vol. 29 (4) (2011) 587–608.
[7] T. Wu, G. Liu, S. Fu, F. Xing, Recent progress of fiber-optic sensors for the structural health monitoring of civil infrastructure, Sensors vol. 20 (16) (2020) 4517.
[8] R. Min, Z. Liu, L. Pereira, C. Yang, Q. Sui, C. Marques, Optical fiber sensing for marine environment and marine structural health monitoring: a review, Opt. Laser Technol. vol. 140 (2021) 107082.
[9] A.S.G. Prasad, S. Asokan, Fiber Bragg grating sensor package for submicron level displacement measurements, Exp. Technol. vol. 39 (6) (2015) 19–24.
[10] R. Li, Y. Tan, T. Li, H. Liu, B. Huang, H. Song, Z. Zhou, L. Cai, A temperature-insensitive FBG displacement sensor with a 10-nanometer-grade resolution, IEICE Electron. Exp. vol. 15 (17) (2018) 20180694.
[11] H. Gnewuch, S. Emil, D.A. Jackson, A.G. Podoleanu, Long range extensometer for civil structure monitoring using fiber Bragg gratings, Meas. Sci. Technol. vol. 16 (2005) 2005–2010.
[12] J. Li, H. Neumann, R. Ramalingam, Design fabrication and testing of fiber Bragg grating sensors for cryogenic long-range displacement measurement, Cryogenics vol. 68 (2015) 36–43.

[13] J. Thomas, T.R. Rajanna, S. Asokan, Temperature compensated FBG displacement sensor for long-range applications, IEEE Sens. Lett. vol. 4 (1) (2020) 5000104.
[14] J.H. Ng, X. Zhou, X. Yang, J. Hao, A simple temperature-insensitive fiber Bragg grating displacement sensor, Opt. Commun. vol. 273 (2) (2007) 398–401.
[15] C. Shen, C. Zhong, Novel temperature-insensitive fiber Bragg grating sensor for displacement measurement, Sens. Actuators A: Phys. vol. 170 (1–2) (2011) 51–54.
[16] C. Zhong, C. Shen, J. Chu, X. Zou, K. Li, Y. Jin, J. Wang, A Displacement Sensor Based on a Temperature-Insensitive Double Trapezoidal Structure With Fiber Bragg Grating, IEEE Sens. J. vol. 12 (5) (2012) 1280–1283.
[17] S. Tao, X. Dong, B. Lai, Temperature-insensitive fiber Bragg grating displacement sensor based on a thin-wall ring, Opt. Commun. vol. 372 (2016) 44–48.
[18] LUNA, Fiber Optic Sensing and Non-Destructing Testing Products. (Accessed 29 June 2023) [online]. Available: https://lunainc.com/product-category/sensing-and-non-destructive-test-products?family=80#category-14.
[19] HBK, newLight: The Easy to Install Optical Sensor for Strain, Tilt, Temperature and Acceleration. (Accessed 29 June 2023) [online]. Available: https://www.hbm.com/index.php?id=4599&L=0&product_type_no=newLight.
[20] W. Liu, Y. Guo, L. Xiong, Y. Kuang, Fiber Bragg grating based displacement sensors: state of the art and trends, Sens. Rev. vol. 39 (1) (2019) 87–98.
[21] C.- Zhu, Y. Zhuang, B. Liu, J. Huang, Review of FIber Optic Displacement Sensors, IEEE Trans. Instrum. Meas. vol. 71 (2022) 7008212.
[22] A. Bernasconi, M. Carboni, L. Comolli, Monitoring of fatigue crack growth in composite adhesively bonded joints using Fiber Bragg Gratings, Procedia Eng. vol. 10 (2011) 207–212.
[23] G. Pereira, L. Mikkelsen, M. McGugan, Crack growth monitoring by embedded optical fibre bragg grating sensors – fibre reinforced plastic crack growing detection, Proc. 3rd Int. Conf. Photonics, Opt. Laser Technol. (OSENS (2015) 133–139. Berlin, Germany (13-15 March 2015.
[24] M. Maheshwari, V.G.M. Annamdas, J.H.L. Pang, A. Asundi, S.C. Tjin, Crack monitoring using multiple smart materials; fiber-optic sensors & piezo sensors, Int. J. Smart Nano Mater. vol. 8 (1) (2017) 41–55.
[25] S.K. Chilelli, J.J. Schomer, M.J. Dapino, Detection of crack initiation and growth using fiber bragg grating sensors embedded into metal structures through ultrasonic additive manufacturing, Sensors vol. 19 (22) (2019) 4917.
[26] M. Mieloszyk, Fatigue crack propagation monitoring using fibre bragg grating sensors, Vib vol. 4 (3) (2021) 700–721.
[27] H. Tsuda, J.-R. Lee, Y. Guan, Fatigue crack propagation monitoring of stainless steel using fiber Bragg grating ultrasound sensors, Smart Mater. Struct. vol. 15 (5) (2006) 1429–1437.
[28] H. Tsuda, J.-R. Lee, Y. Guan, J. Takatsubo, Investigation of fatigue crack in stainless steel using a mobile fiber Bragg grating ultrasonic sensor, Opt. Fiber Technol. vol. 13 (3) (2007) 209–214.
[29] T. Bao, "Distributed Fiber Bragg Grating Sensors for Monitoring Cracks in Concrete," in Thirteenth ASCE Aerospace Division Conference on Engineering, Science, Construction, and Operations in Challenging Environments, and the 5th NASA/ASCE Workshop On Granular Materials in Space Exploration, Pasadena, CA, USA (15–18 April, 2012).
[30] Q. Zhang, Z. Xiong, Crack detection of reinforced concrete structures based on BOFDA and FBG sensors, Shock Vib. vol. 2018 (2018) 6563537.
[31] Y. Yao, S. Li, and Z. Li, "Structural Cracks Detection Based on Distributed Weak FBG" in 26th International Conference on Optical Fiber Sensors, TuE95, Lausanne, Switzerland (24–28 September 2018).
[32] L. Wang, J. Song, Y. Sai, H. Wang, Crack width analysis of reinforced concrete using FBG sensor, IEEE Photon. J. vol. 11 (1) (2019) 6800408.
[33] C. Zhang, Z. Alam, L. Sun, Z. Su, B. Samali, Fibre Bragg grating sensor-based damage response monitoring of an asymmetric reinforced concrete shear wall structure subjected to progressive seismic loads, Struct. Control Health Monit. vol. 26 (3) (2019) e2307.
[34] Y. Ye, S. Hu, X. Fan, J. Lu, Effect of adhesive failute on measurement of concrete cracks using fiber Bragg grating sensors, Opt. Fiber Technol. vol. 71 (2022) 102934.
[35] A. Arêde, P. Costa, A. Costa, C. Costa, and L. Noites, "Monitoring and testing of a new stone masonry arch bridge in Vila Fria, Portugal," in Proceedings of ARCH07 – 5th International Conference on Arch Bridges, pp. 323 330, Funchal, Portugal (12–14 September, 2007).
[36] H. Lima, R. Vicente, R.N. Nogueira, I. Abe, P.S.B. André, C. Fernandes, H. Rodrigues, H. Varum, H.J. Kalinowski, A. Costa, J.L. Pinto, Structural health monitoring of the church of santa casa da misericórdia of aveiro using FBG sensors, IEEE Sens. J. vol. 8 (7) (2008) 1236–1242.
[37] F. Felli, A. Brotzu, D. Pilone, C. Vendittozzi, Use of FBG sensors for monitoring cracks of the equestrian statue of Bartolomeo Colleoni in Venice, Frat. Ed. Integrita Strutt. vol. 8 (30) (2014) 48–54.
[38] A. Coricciati, I. Ingrosso, A.P. Sergi, A. Largo, Application of smart FRT devices for the structural health monitoring of heritage buildings – a case study: the monastery of Sant'Angelo dOcre, Key Eng. Mater. vol. 747 (2017) 448–455.
[39] E. Verstrynge, K.D. Wilder, A. Drougkas, E. Voet, K.V. Balen, M. Wevers, Crack monitoring in historical masonry with distributed strain and acoustic emission sensing techniques, Constr. Build. Mater. vol. 162 (2018) 898–907.
[40] H. Alexakis, A. Franza, S. Acikgoz, and M. DeJong, "Structural Health Monitoring of a masonry viaduct with Fibre Bragg Grating sensors," in IABSE Symposium 2019 Guimarães: Towards a Resilient Built Environment – Risk and Asset Management, Guimarães, Portugal (27–29 March, 2019).
[41] I. Bellagamba, M. Caponero, and M. Mongelli, "Using of fiber optic sensors and 3d photogrammetric reconstruction for crack pattern monitoring of masonry structures at the Aurelian Walls in Rome, Italy," in STREMAH 2019 – 16th International Conference on Studies, Repairs and Maintenance of Heritage Architecture, pp. 457–465, Seville, Spain (7–9 October, 2019).
[42] H. Gupta, D. Ghosh, A.K. Mittal, Monitoring of settlement in masonry arch using FBG sensor (10-12 December, NDE 2020 – Virtual Conf. Exhib. vol. 26 (4) (2020) (10-12 December.
[43] M.J.B. Neto, "*James Murphy e o Restauro do Mosteiro de Santa Maria da Vitória no Século XIX*," Teoria da Arte, Lisbon, Portugal: Editorial Estampa, 1997.
[44] M. Solla, L.M.S. Gonçalves, G. Gonçalves, C. Francisco, I. Puente, P. Providência, F. Gaspar, H. Rodrigues, A building information modeling approach to integrate geomatic data for the documentation and preservation of cultural heritage, Remote Sens vol. 12 (24) (2020) 4028.
[45] R. Kashyap. Fiber Bragg Gratings, 2nd ed..,, San Diego, CA, USA: Academics Express, 2009.
[46] L. Pereira, R. Min, G. Woyessa, O. Bang, C. Marques, H. Varum, P. Antunes, Interrogation method with temperature compensation using ultra-short fiber bragg gratings in silica and polymer optical fibers as edge filters, Sensors vol. 23 (1) (2023) 23.
[47] L. Pereira, C. Marques, R. Min, G. Woyessa, O. Bang, H. Varum, P. Antunes, Bragg gratings in ZEONEX microstructured polymer optical fiber with 266-nm Nd:YAG laser, IEEE Sens. J. vol. 23 (9) (2023) 9308–9316.
[48] C.A. Harper. Modern Plastics Handbook, 1st ed., McGraw Hill, New York, NY, USA, 2000.
[49] D.G. LeGrand, J.T. Bendler. Handbook of Polycarbonate Science and Technology, 1st ed., Marcel Dekker, New York, NY, USA, 2000.
[50] S. Bäumer. Handbook of Plastic Optics, 2nd ed., Wiley-VCH, Weinheim, Germany, 2010.
[51] A. Suvorova, E. Tchirkova, Optical properties of plasticized polycarbonate, Polym. Int. vol. 53 (2) (2004) 153–155.

Luís Pereira received the Master's degree in Physics Engineering in 2017, from the University of Aveiro, Portugal. His specialization and interests are focused on the production and investigation of Fiber Bragg Gratings in silica and polymer optical fibers using UV laser systems, on the development of optical fiber sensors and sensing networks for static and dynamic measurements and on the data acquisition and processing. From 2017 to 2019 he was a Research Fellow with the I3N-Aveiro (Institute of Nanostructures, Nanomodelling and Nanofabrication). He is currently attending the Physics Engineering doctoral program at the I3N & Physics Department of the University of Aveiro, and his research includes the study, simulation, and development of optical fiber devices, in silica and polymer fibers, for filtering and sensing applications in Structural Health Monitoring.

Inês Bourgeois completed her Bachelor's degree in Heritage Rehabilitation, at the University of Aveiro, in 2019. That same year, she began her Master's degree in Heritage Rehabilitation at the University of Aveiro and joined the Scientific Initiation Program of the RIsks and Sustainability in Construction (RISCO) research unit, in the "Intervention in Reinforced Concrete Structures" project. She completed her Master's degree in 2021, and right after that, began the Doctoral Program in the field of cultural heritage, about the integrated characterization and monitoring of heritage buildings - application to the Monastery of Santa Maria da Vitória.

Hugo Rodrigues is Associate Professor at the Civil Engineering Department of the University of Aveiro. He completed his PhD in Civil Engineering at the University of Aveiro, in 2012. His specialization is focused in assessing the seismic behavior of existing structures. He participated and collaborated in research and development projects with several national and international institutions. His main research interests are related to Building Rehabilitation, Structural Monitoring and Seismic Safety, including experimental and numerical activities, and is currently a member of RIsks and Sustainability in Construction (RISCO) research unit. He co-authored several publications in international magazines, and in national and international conferences.

Humberto Varum is full professor at the Faculty of Engineering of the University of Porto, Portugal. He is integrated member of CONSTRUCT research unit: Institute of R&D in Structures and Construction. He has been Seconded National Expert to the ELSA laboratory, Joint Research Centre, European Commission, Italy, in the period July 2009 to August 2010. Since May 2015, he is member of the directorate body of the Construction Institute from the University of Porto, and President since May 2019. He was member of the Project Team 2 for the development of the 2nd generation of EN Eurocodes (SC8. T2 - material dependent sections of EN 1998–1). He is member of the National Committee of the International Council on Monuments and Sites (ICOMOS), since 2009, and Expert Member of the ICOMOS's International Scientific Committee of Earthen Architectural Heritage (ISCEAH). He has participated to post-earthquake field reconnaissance missions, in particular in L'Aquila (Italy, 2009), Lorca (Spain, 2011), Emilia-Romagna (Italy, 2012), Gorkha (Nepal, 2015) and Puebla (Mexico, 2017). His main research interests include: assessment, strengthening and repair of structures, earthquake engineering, historic constructions conservation and strengthening.

Paulo Fernando da Costa Antunes received the Ph.D. in Physics Engineering in 2011 from the Universidade de Aveiro, Portugal. Currently he is an Assistant professor at the Physics Department of the Aveiro University, Portugal. As a researcher, he is also with the I3N-Aveiro (Institute of Nanostructures, Nanomodelling and Nanofabrication) and the Instituto de Telecomunicaç ões. His research interests include the study and simulation of optical fiber sensors based on silica and polymeric fibers, for static and dynamic measurements, data acquisition, optical transmission systems and sensor networks for several applications, including medical applications and structural health monitoring. He

authored or co-authored more than 200 international journal, book chapter and conference technical papers with emphasis on optical sensing devices and applications.